



OPEN

Preparation of Few-Layer Bismuth Selenide by Liquid-Phase-Exfoliation and Its Optical Absorption Properties

Liping Sun¹, Zhiqin Lin¹, Jian Peng¹, Jian Weng^{1,3}, Yizhong Huang² & Zhengqian Luo²

SUBJECT AREAS:

LASERS, LEDS AND LIGHT
SOURCES

FIBRE LASERS

SYNTHESIS AND PROCESSING

Received
4 November 2013Accepted
8 April 2014Published
25 April 2014

Correspondence and
requests for materials
should be addressed to
J.W. (jweng@xmu.
edu.cn) or Z.Q.L.
(zqluo@xmu.edu.cn)

¹Department of Biomaterials, College of Materials, Xiamen University, Xiamen 361005, China, ²Institute of Optoelectronic Technology, Department of Electronic Engineering, Xiamen University, Xiamen 361005, China, ³ShenZhen Research Institute of Xiamen University, Shenzhen 518057, China.

Bismuth selenide (Bi_2Se_3), a new topological insulator, has attracted much attention in recent years owing to its relatively simple band structure and large bulk band gap. Compared to bulk, few-layer Bi_2Se_3 is recently considered as a highly promising material. Here, we use a liquid-phase exfoliation method to prepare few-layer Bi_2Se_3 in N-methyl-2-pyrrolidone or chitosan acetic solution. The resulted few-layer Bi_2Se_3 dispersion demonstrates an interesting absorption in the visible light region, which is different from bulk Bi_2Se_3 without any absorption in this region. The absorption spectrum of few-layer Bi_2Se_3 depends on its size and layer number. At the same time, the nonlinear and saturable absorption of few-layer Bi_2Se_3 thin film in near infrared is also characterized well and further exploited to generate laser pulses by a passive Q-switching technique. Stable Q-switched operation is achieved with a lower pump threshold of 9.3 mW at 974 nm, pulse energy of 39.8 nJ and a wide range of pulse-repetition-rate from 6.2 to 40.1 kHz. Therefore, the few-layer Bi_2Se_3 may excite a potential applications in laser photonics and optoelectronic devices.

Topological insulators (TIs) as interesting insulators now have become the rising star in physics, chemistry and materials fields because they are insulating in the bulk phase but possess exotic metal surface state as a result of the combination of spin-orbit interactions and time-reversal symmetry^{1–3}. In the past few years, some research groups^{4–6} achieved great success in the prediction and experimental confirmation of TIs, including Bi_2Se_3 , Bi_2Te_3 and Sb_2Te_3 , which have a large band gap and a single Dirac cone. Especially, the remarkable band gap of Bi_2Se_3 is approximately up to 0.3 eV (equivalent to 3600 K) that is much larger than the room temperature energy scale⁴. It means that Bi_2Se_3 is able to exhibit topological insulator behavior at room temperature, which is considered as a promising topological system with a good application prospect⁷. Recently, most researchers paid attention to the physical basis^{8–10}, synthesis method^{11,12} and exploration of the nanostructure^{13–15} of TIs. However, it is worth noting that topological properties of Bi_2Se_3 as three-dimensional (3D) TIs are often covered up by the bulk state due to high carrier density^{5,16}. Therefore, it is necessary to prepare two-dimensional (2D) Bi_2Se_3 from its 3D bulk materials in order to acquire the superior performance for some potential applications.

Bi_2Se_3 possesses stacked layers of laminated structure that are held together by weak van der Waals interactions. Each layer is one quintuple layer (QL) and the five atoms are covalently bonded together along the z axis in the order of Se-Bi-Se-Bi-Se (Fig. 1a). The thickness of each layer is about 0.96 nm¹⁷. It is possible to exfoliate bulk Bi_2Se_3 into few-layer nanosheets due to the weak interaction between layers. Up to date, bottom-up synthesis and top-down exfoliation are two main methods to prepare 2D nanomaterials³. Bottom-up synthesis approach is used to obtain single-layer or fewer layer 2D nanomaterials by a chemical reaction from the atomic or molecular scale synthesis^{18–21}. 3D materials held together by weak van der Waals forces can be exfoliated into thin flakes by the methods of mechanical or chemical exfoliation^{22–24}, which is a top-down process. Therefore, it is possible to obtain few-layer QLs from bulk Bi_2Se_3 with “graphene-inspired” exfoliation methods because bulk Bi_2Se_3 possesses the graphene-like layered structure. Liquid-phase exfoliation has been used to produce single-layer or few-layer graphene because it is easier and more convenient than other methods. Furthermore, the as-obtained graphene could form colloidal dispersions in solvents^{24,25}. Therefore, we attempted to exfoliate bulk Bi_2Se_3 by liquid-phase exfoliation method to prepare few-layer Bi_2Se_3 in solutions.

As a new type of Dirac material, TIs with the unique energy-band structure can induce some fantastically electronic and optical properties²⁶, opening up many new applications, such as superconductors²⁷ and ultrafast lasers^{28,29}. Nowadays, these researches are focused on pulsed lasers due to their versatile applications in range

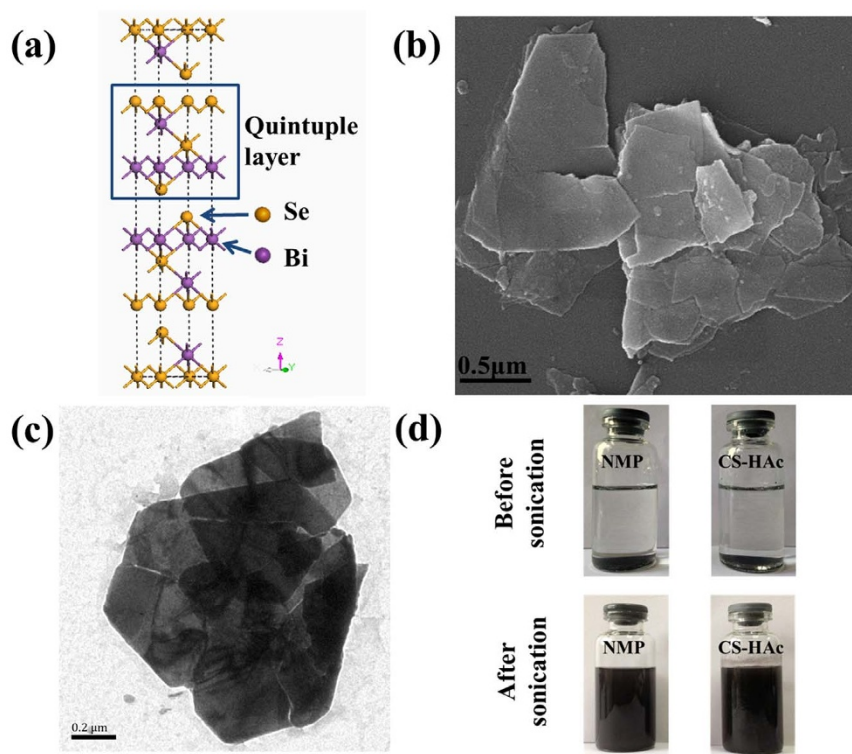


Figure 1 | Preparation and exfoliation of as-synthesized bulk Bi_2Se_3 . (a) Schematic of rhombohedral layer structure held together by weak van der Waals interactions in Bi_2Se_3 . Each QL consists of five covalently bonded atomic sheets along the z axis in the order of Se-Bi-Se-Bi-Se. (b), (c) SEM and TEM images of as-synthesized bulk Bi_2Se_3 . (d) Photographs of Bi_2Se_3 dispersed in NMP and CS-HAc before and after sonication.

finding, medicine, laser processing, remote sensing and telecommunications³⁰. In the field of pulsed lasers, passive Q-switched fiber laser for generating short and large-energy laser pulse is one of most effective ways because of their significant advantages of compactness, simplicity, and flexibility in design³¹. The key element in the passive Q-switched fiber laser is an excellently saturable absorber. Therefore, researchers have never stopped to seek for new saturable absorbers (e.g. semiconductor³², carbon nanotubes³³, graphene^{33,34}). Compared with bulk materials^{28,29}, one can expect that the few-layer nanomaterials would possess the more excellent performance of saturable absorption, and could be a potentially saturable absorber. Therefore, we are strongly motivated to develop the pulsed fiber lasers Q-switched with few-layer Bi_2Se_3 as the saturable absorber.

Here, N-methyl-2-pyrrolidone (NMP), the more promising organic solvent to exfoliate 2D layered materials²⁴, is used to exfoliate bulk Bi_2Se_3 for producing few-layer Bi_2Se_3 (Supplementary Fig. S1). Another is chitosan acetic solution (CS-HAc), which possesses the low-toxic, good-biocompatible and environmentally friendly properties³⁵. Meanwhile, we also investigated the optical absorption characterization of as-prepared few-layer Bi_2Se_3 dispersed in solvents in visible light region, and saturable-absorption performance of few-layer Bi_2Se_3 thin film in near infrared region. At last, few-layer Bi_2Se_3 was successfully used as the new fiber-compatibly saturable absorber to attain passive Q-switched fiber laser at 1.53 μm wavelength.

Results

Preparation and exfoliation of bulk Bi_2Se_3 . Bulk Bi_2Se_3 was prepared by hydrothermal synthesis and characterized by X-ray diffraction (XRD, Supplementary Fig. S2a). All the labeled peaks can be readily indexed to rhombohedral Bi_2Se_3 (JCPDS no. 89-2008). The scanning electron microscope (SEM) image in Fig. 1b and transmission electron microscope (TEM) image in Fig. 1c show that the as-synthesized bulk Bi_2Se_3 exhibits sheet-like structure with a wide size distribution, and is easily to aggregate together.

The thickness of as-synthesized bulk Bi_2Se_3 is about 40–100 nm determined by atomic force microscopy (AFM) (Supplementary Fig. S2c and d).

We further exfoliated as-synthesized bulk Bi_2Se_3 with solution-phase exfoliation method, which is similar to the exfoliation of graphite in NMP and CS-HAc³⁵. The as-synthesized Bi_2Se_3 powders were insoluble in two solvents before sonication (Fig. 1d). After sonication of 30 h, the colors of two solutions were deepened, which means that the exfoliated Bi_2Se_3 had been dispersed in these solvents. We also investigated the exfoliation of as-synthesized bulk Bi_2Se_3 in other solvents (Supplementary Fig. S3). The result shows that NMP and CS-HAc are the optimal solvents to exfoliate as-synthesized bulk Bi_2Se_3 . Therefore, NMP and CS-HAc are selected to investigate the exfoliation of bulk Bi_2Se_3 . We further investigated the effect of sonication time on exfoliation of bulk Bi_2Se_3 (Supplementary Fig. S4). With increasing ultrasonic time, the color of CS-HAc was deepened, but color is already deep dark in NMP at 2 h, which reveals a better exfoliating effect in NMP. Longer ultrasonic time should produce higher concentration of few-layer Bi_2Se_3 . However, it needs more power and time. Therefore, we chose 30 h as the appropriately ultrasonic time because Bi_2Se_3 has already been well dispersed in these two solvents, meeting the requirement of following experiments in this study. The exfoliated Bi_2Se_3 also presented the Tyndall effect of the colloidal suspension (Supplementary Fig. S5). The result shows that the colloidal suspension of exfoliated Bi_2Se_3 in the two solvents is stable.

Characterization of few-layer Bi_2Se_3 . The TEM image (Fig. 2a) of exfoliated Bi_2Se_3 showed that the as-obtained few-layer Bi_2Se_3 was extremely thin 2D flake. According to the selected area electron diffraction (SAED) pattern (Fig. 2b), it could be indexed as a 6-fold symmetry [001] zone axis pattern, which is consistent with the layered structure along the z axis. Also, it revealed the single-crystalline nature of the thin 2D flake. Furthermore, the distance

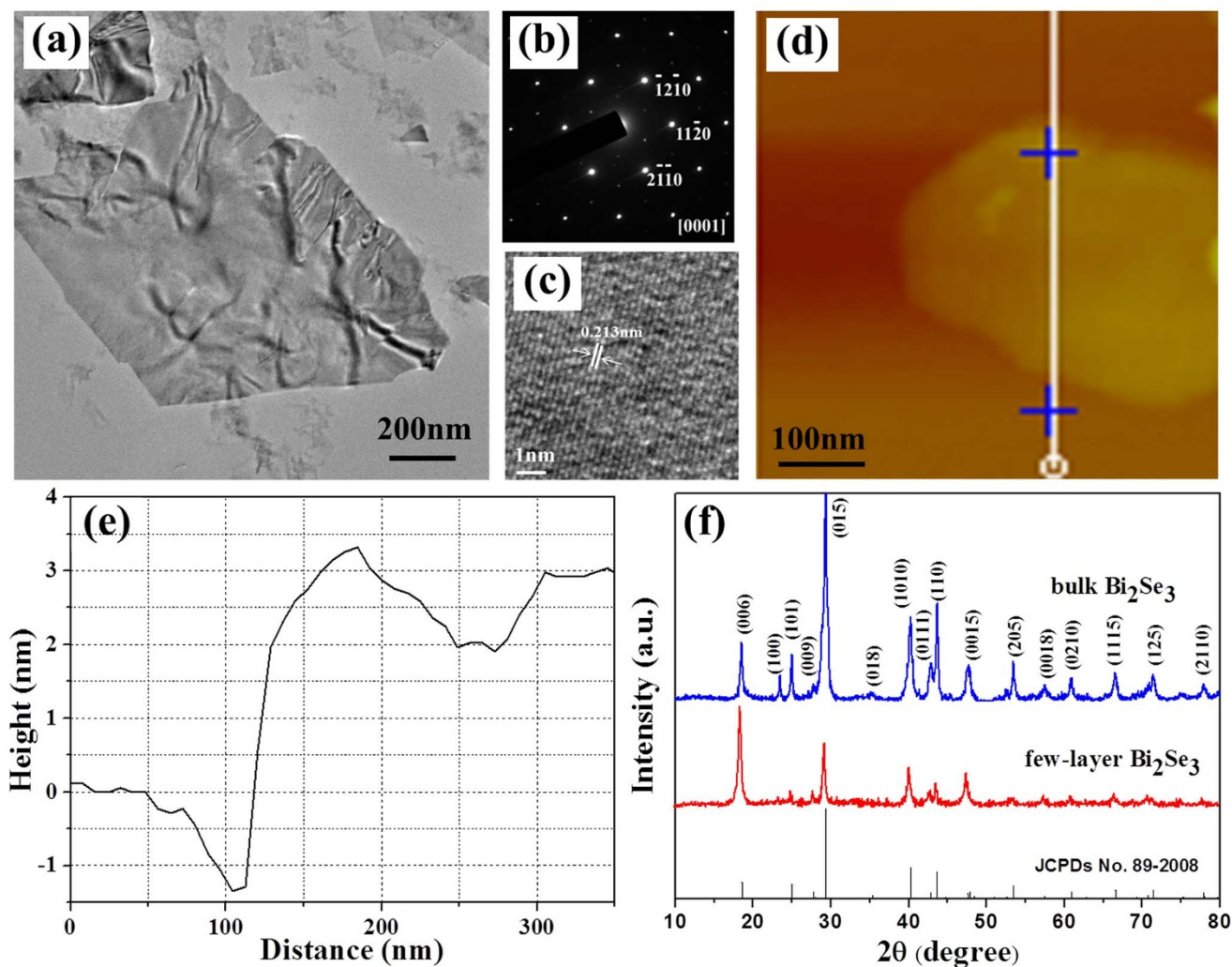


Figure 2 | Confirmation of few-layer Bi_2Se_3 exfoliated in NMP. (a) TEM image of few-layer Bi_2Se_3 . (b) SAED pattern of few-layer Bi_2Se_3 . (c) HRTEM image of few-layer Bi_2Se_3 . (d), (e) AFM image and the corresponding height profile of few-layer Bi_2Se_3 . (f) XRD patterns of few-layer Bi_2Se_3 and bulk Bi_2Se_3 .

between the adjacent hexagonal lattice fringes investigated by the high-resolution TEM (HRTEM) is 0.213 nm for Bi_2Se_3 (Fig. 2c), which is consistent with the lattice space of the (110) plane. The AFM image (Fig. 2d) also shows that the exfoliated Bi_2Se_3 is a flake structure and its thickness is about 3–4 nm (Fig. 2e), which nearly equals to 4 layers of Bi_2Se_3 ¹⁷. The XRD pattern (Fig. 2f) of few-layer Bi_2Se_3 showed a high [006] orientation and some characteristic peaks disappeared compared to bulk Bi_2Se_3 , which indicates that bulk Bi_2Se_3 had been successfully exfoliated as we expected. At the same time, the bulk Bi_2Se_3 has successfully been exfoliated to few-layer Bi_2Se_3 in CS-HAc (Supplementary Fig. S6). Besides, Raman spectrum was also used to further confirm the exfoliation of Bi_2Se_3 (Supplementary Fig. S7). The A mode of few-layer Bi_2Se_3 produced a red shift compared to that of bulk Bi_2Se_3 , which could be attributed to the phonon softening^{36,37}. Therefore, we successfully prepared few-layer Bi_2Se_3 using the solution-phase exfoliation method.

Optical absorption characterization of few-layer Bi_2Se_3 . The optical absorption properties of few-layer Bi_2Se_3 were firstly investigated with ultraviolet-visible (UV-vis) spectra. Interestingly, we found that the dispersion solutions of few-layer Bi_2Se_3 produced a broad absorption in the visible light region compared to as-synthesized bulk Bi_2Se_3 (Fig. 3a). The UV-vis spectrum of as-synthesized bulk Bi_2Se_3 showed a nearly straight line without any absorption peak in

the visible light region. However, few-layer Bi_2Se_3 displayed an absorption band at about 552 nm in CS-HAc and 574 nm in NMP, respectively. The appearance of absorption band after exfoliation is remarkable, which might be due to the exfoliation of bulk Bi_2Se_3 into nanosheets with a few nanometers thickness. The absorption also increases gradually as the sonication time extended (Fig. 3b and c), which reveals that more few-layer Bi_2Se_3 would be obtained with increasing sonication times. The result further suggests that the absorption would be resulted from few-layer Bi_2Se_3 .

We further investigate the effect of size and thickness on absorption property. After sonication in NMP, few-layer Bi_2Se_3 was separated in different centrifugal speeds (Fig. 4a). The size distribution and corresponding height profile of few-layer Bi_2Se_3 collected at three centrifugation speeds were distinguishing. With centrifugal speed increasing, the size of few-layer Bi_2Se_3 was decreased from 500 to 100 nm and the thickness was also decreased from 10 to 2 nm, and the maximal absorption wavelength was blue-shifted from 613 to 459 nm (Fig. 4b). The similar result is also obtained in CS-HAc (Supplementary Fig. S8 and S9). The result further suggests that the broad absorption in the visible light region would be resulted from few-layer Bi_2Se_3 but not from bulk Bi_2Se_3 .

To further investigate the optical absorption properties of few-layer Bi_2Se_3 , we used a spin-coating method to prepare $\text{Bi}_2\text{Se}_3/\text{NMP}$ (few-layer Bi_2Se_3 exfoliated in NMP) and $\text{Bi}_2\text{Se}_3/\text{CS-HAc}$

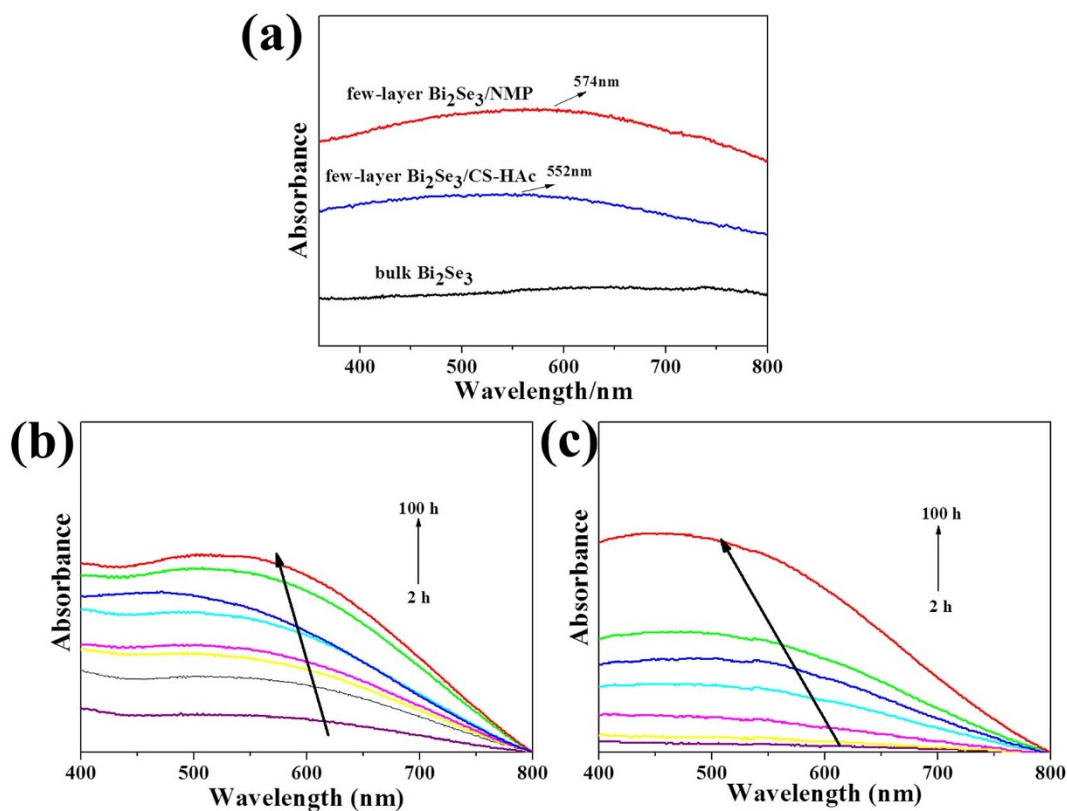


Figure 3 | UV-vis absorption spectra of few-layer Bi₂Se₃. (a) UV-vis absorption spectra of as-synthesized bulk and few-layer Bi₂Se₃ suspension. (b) UV-vis absorption spectra of few-layer Bi₂Se₃ suspension prepared with different sonication times in NMP. (c) UV-vis absorption spectra of few-layer Bi₂Se₃ suspension prepared with different sonication times in CS-HAc. The upper part of resulting suspension of each sample after sonication was collected, and then centrifuged for 30 min at 1000 rpm to receive the supernatant as the measurement solution.

(few-layer Bi₂Se₃ exfoliated in CS-HAc) thin films on quartz plate, respectively. As shown in Fig. 5a, we measured the linear absorption spectra of the two films by a spectrophotometer scanning from 300 to 2000 nm. One can clearly see that both of the films have the relatively flat transmission curves in the UV-to-near infrared (NIR) region, e.g. the transmittance of Bi₂Se₃/NMP varies only from 0.67 to 0.84 in the broad wavelength range of 350 ~ 2000 nm. It indicates that the few-layer Bi₂Se₃ would be a promising broadband optical material. In order to compare the nonlinear absorption of our few-layer Bi₂Se₃ with that of bulk Bi₂Se₃ (>50 layers) previously reported^{38,39}, we also used the same Z-scan technique to measure the nonlinear transmission responses of the two few-layer Bi₂Se₃ films. When the two samples were strongly excited by a femtosecond Ti: sapphire laser with the highest optical intensity of 2.6 GW/cm² (Fig. 5b and c), the open-aperture Z-scan transmission curves of Bi₂Se₃/NMP and Bi₂Se₃/CS-HAc were obtained, respectively. One can obviously see that the two samples possess the saturable absorption, i.e. the optical transmittance is different under differently optical intensity. The modulation depths (δT) are 3.8% for Bi₂Se₃/NMP and 3.7% for Bi₂Se₃/CS-HAc, respectively, which is comparable to that of graphene^{40,41}. Furthermore, by carefully fitting the curves in Fig. 5b and 5c, the produced saturable intensities (I_{sa}) are 53 MW/cm² for Bi₂Se₃/NMP and 41 MW/cm² for Bi₂Se₃/CS-HAc, respectively. It is very interesting that the I_{sa} values are much less than that of bulk Bi₂Se₃ reported previously^{38,39}, mainly benefiting from the few-layer structure of exfoliated Bi₂Se₃. In the field of passive Q-switched or mode-locked lasers, the lower I_{sa} of saturable absorber, the easier the start of Q-switching/mode-locking operation is, implying that few-layer Bi₂Se₃ might be very helpful for developing the low-threshold Q-switched/mode-locked lasers.

Generation of Q-switched laser pulses using the saturable absorption of few-layer Bi₂Se₃. As well as known, the optically saturable absorption can be used to efficiently generate the laser pulses by the passive Q-switching or mode-locking techniques^{42,43}. The lower I_{sa} of few-layer Bi₂Se₃ may be very helpful for developing the low-threshold Q-switched/mode-locked lasers. In this section, to testify the performance of few-layer Bi₂Se₃, we will exploit the saturable absorption of few-layer Bi₂Se₃ to passive Q-switch erbium-doped fiber laser (EDFL) for generating laser pulses. Supplementary Fig. S10 shows the experimental setup of Q-switched EDFL using few-layer Bi₂Se₃ as a saturable absorber. In order to clearly evaluate the significance of few-layer Bi₂Se₃ to Q-switching operation, we purposely performed the following control experiments. At first, when as-synthesized bulk Bi₂Se₃ was deliberately inserted into the laser cavity, we found that the Q-switching operation at 1530.2 nm was extremely unstable with a large pulse-intensity and repetition-rate fluctuation (see the Supplementary Fig. S11 for more details). Moreover, the Q-switching operation has a high pump threshold of 22.1 mW, a broad pulse duration of 22.8 μ s and a small operating range of pump power (22.1 ~ 67.5 mW). In contrast, a very stable Q-switching operation was produced when the few-layer Bi₂Se₃ was placed in the laser cavity to replace as-synthesized bulk Bi₂Se₃ as followed.

As increasing the pump power, we found that the laser with few-layer Bi₂Se₃ as saturable absorber reached its threshold at the pump power of 9.3 mW only, and the stable Q-switching operation occurred simultaneously. The pump threshold for Q-switching is much lower than that of as-synthesized bulk Bi₂Se₃ (22.1 mW), and other saturable absorber-based pulsed EDFLs reported previously^{29,38,39}, mainly benefiting from the lower I_{sa} of few-layer

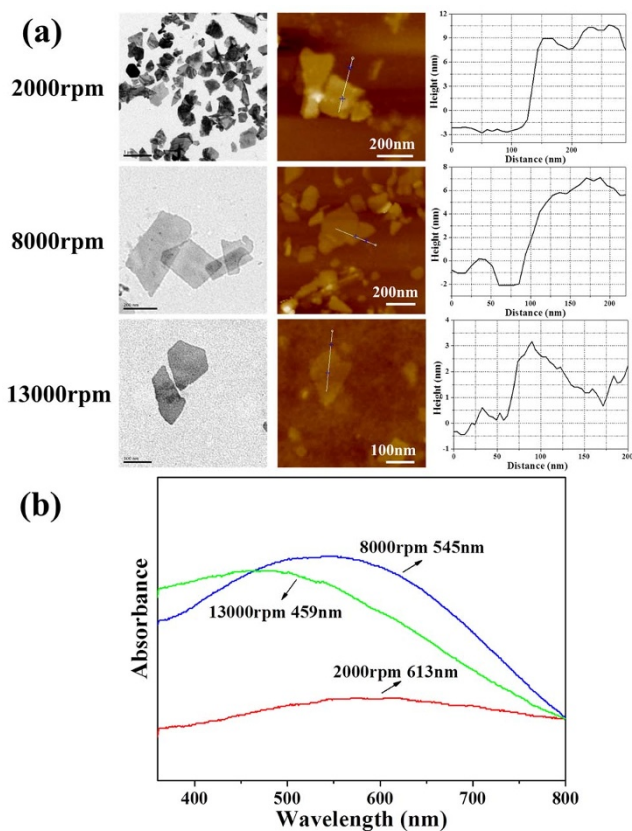


Figure 4 | Few-layer Bi_2Se_3 in NMP collected in different centrifugal speeds. (a) TEM and AFM images, and the corresponding height profiles of few-layer Bi_2Se_3 in NMP collected in different centrifugal speeds. Firstly, the stock solution was centrifuged at 2000 rpm for 30 min, and the precipitate was collected as sample one (top). Then, the remaining supernatant was centrifuged at 8000 rpm for 20 min, and the precipitate was collected as sample two (middle). At last, the supernatant collected in second step was further centrifuged at 13000 rpm for 12 min, and the precipitate was collected as sample three (bottom). (b) UV-vis absorption spectra of few-layer Bi_2Se_3 in NMP. The absorption band was blue-shifted with decreasing thickness and size of few-layer Bi_2Se_3 .

Bi_2Se_3 . Fig. 6 summarizes the output characteristics of the Q-switched pulses. Fig. 6a and 6b give the typical oscilloscope trace of the Q-switched pulse trains and the single pulse envelope at the pump power of 87.2 mW, respectively. The Q-switching pulse output with the repetition rate of 23.8 kHz was stable, and no significant pulse jitter was observed on the oscilloscope. The measured

single-pulse envelope shows the good symmetry and has the pulse duration of 5.4 μs . The typical laser spectrum of the Q-switching operation depicted in Fig. 6c has the central wavelength of 1530.3 nm with the 10-dB bandwidth of 2.2 nm. As usually observed in Q-switched fiber lasers⁴⁴, the sideband structure appeared in the optical spectrum was due to the multimode oscillation and the cavity perturbations of Q-switching⁴⁴. As shown in Fig. 6d, we also measured the RF output spectrum of Q-switching pulses at the same pump power of 87.2 mW. The pulse repetition rate is 23.8 kHz. The RF signal-to-noise ratio is more than 50 dB, and the 20-dB RF linewidth is less than 10 Hz (limited by the RF resolution bandwidth of 10 Hz), further indicating the good stability of the Q-switching operation. Moreover, the stability of the Q-switching is excellent in our testing period of 4 h, and the stable Q-switching is available in the large range of pump power (9.3 ~ 150.1 mW), which is superior to that of bulk Bi_2Se_3 (22.1 ~ 67.5 mW). Fig. 6e plots the pulse repetition rate and the pulse energy as a function of the pump power. As increasing the pump power from 9.3 to 150.1 mW, one can see that: 1) the pulse repetition rate linearly increases from 6.2 to 40.1 kHz; and 2) the pulse energy monotonically increases in the lower pump power, but slightly saturates after exceeding the pump power of 100 mW. The maximum pulse energy obtained in our experiment is 39.8 nJ, corresponding to the average output power of 1.6 mW at the pump power of 150.1 mW. In addition, we also recorded the evolution of pulse duration in different pump powers. As shown in Fig. 6f, the pulse duration can be significantly narrowed from 24.0 to 4.9 μs with the increase of pump power. The pulse duration might be further reduced by shortening the cavity length and optimizing the cavity loss⁴⁵.

Discussion

In this work, we attempted to exfoliate as-synthesized bulk Bi_2Se_3 for preparing few-layer Bi_2Se_3 by liquid-phase exfoliation method, and the result shows that it is viable. In the process of preparation, ten solvents were used to exfoliate Bi_2Se_3 with same ultrasonic time and concentration in order to find the optimal solvents to exfoliate Bi_2Se_3 . With the aid of ultrasound wave, few-layer Bi_2Se_3 has successfully been prepared in NMP and CS-HAc. The exfoliation of as-synthesized bulk Bi_2Se_3 is attributed to the energy provided by the ultrasound wave which overcomes the van der Waals force between Bi_2Se_3 QLs. With the increasing of ultrasonic time, higher concentration of few-layer Bi_2Se_3 was produced. However, the increasing amount of few-layer Bi_2Se_3 is not obvious after 30 h. Considering the efficiency of preparation, 30 h is selected as the appropriate ultrasonic time to prepare few-layer Bi_2Se_3 . In NMP solvent, many materials held by van der Waals forces could be exfoliated to produce 2D nanosheets due to its appropriate surface tension⁴⁶. Bi_2Se_3 has a similar structure held together via van der Waals forces between QLs, so it is possible

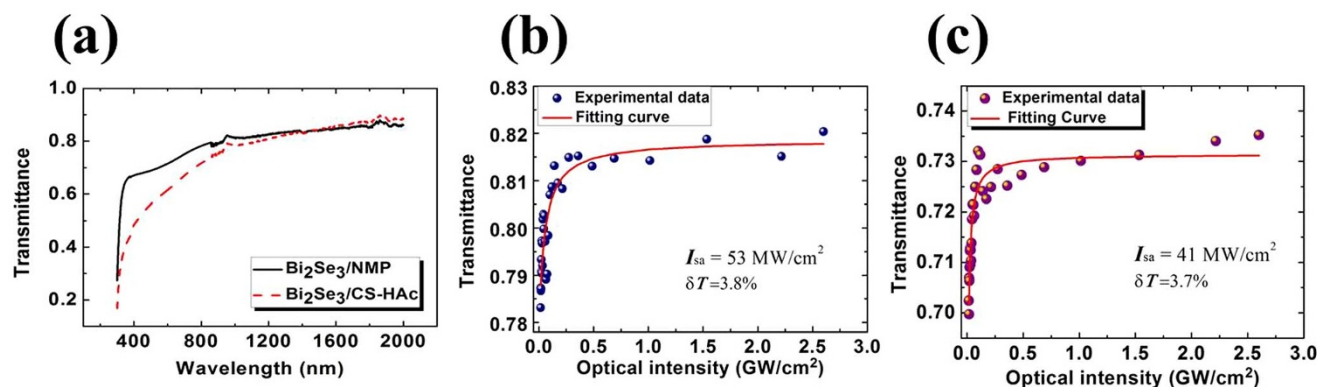


Figure 5 | Optical absorption of few-layer Bi_2Se_3 . (a) The linear absorption of few-layer Bi_2Se_3 . (b) The nonlinear optical absorption (i.e. saturable absorption) of $\text{Bi}_2\text{Se}_3/\text{NMP}$. (c) The nonlinear optical absorption (i.e. saturable absorption) of $\text{Bi}_2\text{Se}_3/\text{CS-HAc}$.

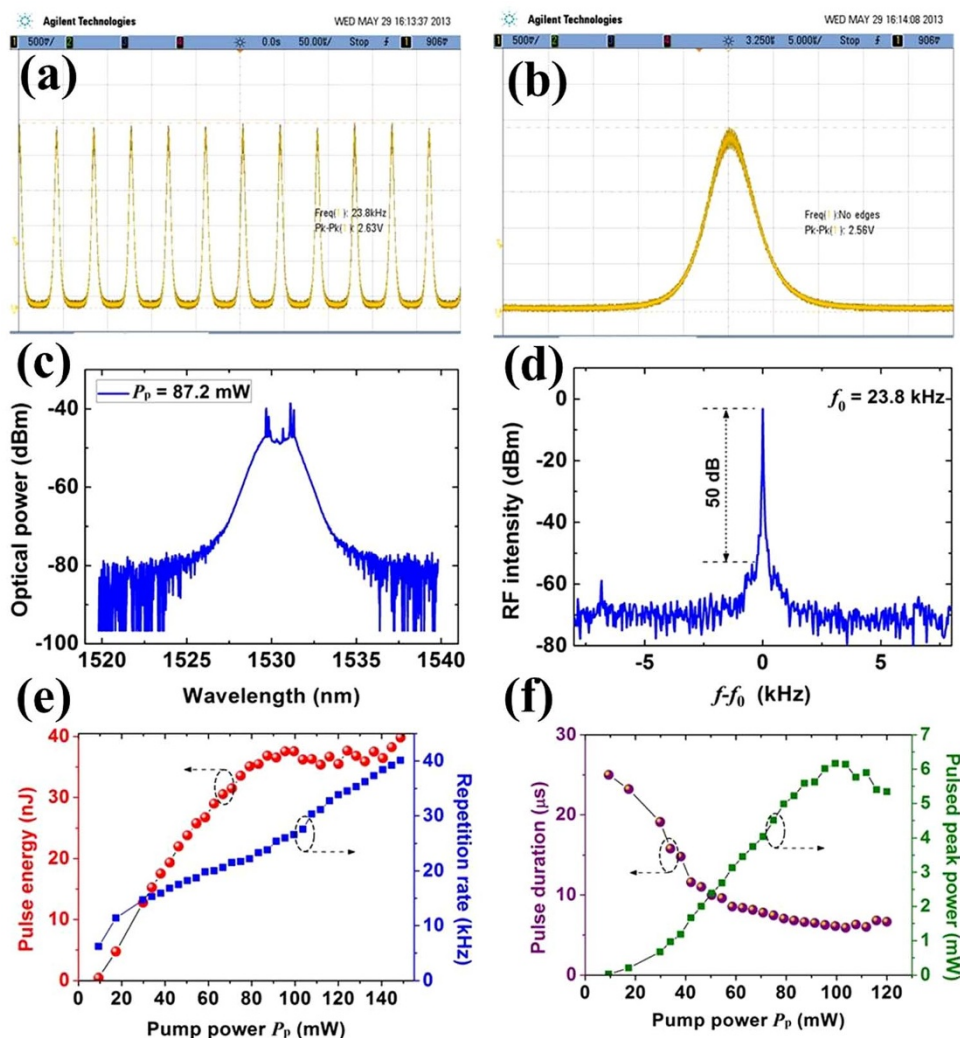


Figure 6 | Performance of few-layer Bi₂Se₃ to passively Q-switch erbium-doped fiber laser. (a) The typical oscilloscope trace of Q-switched pulses at the pump power of 87.2 mW. (b) The single pulse envelope. (c) The typical optical spectrum of Q-switching operation. (d) The RF output spectrum. (e) The pulse repetition rate and the pulse energy vs the pump power. (f) The pulse duration as a function of the pump power.

to obtain few-layer Bi₂Se₃ after sonication in NMP. Really, the expected results have been obtained as we suppose so. Another aqueous surfactant solution, CS-HAc, was also used to prepare few-layer Bi₂Se₃ through hydrophobic interaction of main chains of chitosan and the surface of Bi₂Se₃. Few-layer Bi₂Se₃ can stably be dispersed in chitosan dispersion, which is due to the electrostatic repulsion³⁵ between NH₄⁺ in the side chains of chitosan adsorbed on the surface of Bi₂Se₃. Therefore, liquid-phase-exfoliation of as-synthesized bulk Bi₂Se₃ allows production of few-layer Bi₂Se₃ suspensions in NMP or CS-HAc, which might be a simple and convenient method to prepare few-layer Bi₂Se₃ for further investigating its properties and exploring the promising applications.

The optical absorption spectrum of few-layer Bi₂Se₃ in solution exhibits a strong absorption band in the visible light region, which is different from as-synthesized bulk Bi₂Se₃ without any absorption peak in this region. The few-layer Bi₂Se₃ with a small size can be considered as a “quantum dot” that would result in quantum confinement, leading to resonance that can be tuned with size. Therefore, the optical absorption of few-layer Bi₂Se₃ is size-dependent (Fig. 4). The products in this study consist of nanosheets with different sizes and thicknesses, and it is difficult to prepare the sample of fixed size with different thickness or fixed thickness with different sizes. Therefore, for systematic and in-depth investigating the effect of thickness and size on the optical absorption of few-layer Bi₂Se₃, it

is necessary to synthesize nanosheets that are monodispersed in both size and thickness, but it remains a challenge by liquid-phase-exfoliation method at this stage.

The blue-shift of UV-vis absorption of few-layer Bi₂Se₃ with its size decreasing is similar to the results for many semiconductor nanoparticles⁴⁷, which the small dimensions result in differently physical properties compared with their corresponding bulk materials. Therefore, we also studied the optical band gap (E_g) of few-layer Bi₂Se₃ according to their optical absorption spectra in solution. The optical absorption properties of few-layer Bi₂Se₃ with different size and thickness in solutions were further investigated in UV-Vis-NIR spectral region (Supplementary Fig. S12 and 13). There is not obvious absorption peak in NIR region. The recorded absorption spectra were mathematically processed to acquire the values of E_g ⁴⁸. The optical absorption is calculated using the following equation:

$$(\alpha h\nu)^n = B(h\nu - E_g) \quad (1)$$

where α is the absorption coefficient, h is Planck constant, ν is the frequency of photon, E_g is the band gap and B is a constant. For the direct band gap semiconductor Bi₂Se₃, n is 2. The $(\alpha h\nu)^2$ vs. $h\nu$ curves for all samples were shown in Supplementary Fig. S12 and 13. The E_g of few-layer Bi₂Se₃ with different sizes and thicknesses obtained by different centrifugation speeds in NMP were determined by extrapolating the straight portion of the plot to the energy axis. The E_g



were 1.22 eV for 2000 rpm, 1.39 eV for 8000 rpm and 1.50 eV for 13000 rpm (more details in supplementary Table S1 and S2), respectively, which is higher than that of as-synthesized bulk Bi_2Se_3 (1.08 eV). Meanwhile, the E_g of few-layer Bi_2Se_3 increases with the centrifugation speed increasing (size and thickness of few-layer Bi_2Se_3 decreasing), which indicates a blue-shift phenomenon. The reason for this larger E_g of few-layer Bi_2Se_3 might be due to the well-known quantum confinement effect by shifting the conduction and valence band edges in opposite directions^{49–51}. It is worth noting that the E_g of as-synthesized bulk Bi_2Se_3 is larger than the theoretical value (0.3 eV) calculated by first-principle electronic structure. The reason is that the as-synthesized “bulk” Bi_2Se_3 with a thickness of 40–100 nm and a size of 100–500 nm (Supplementary Figure S2) is smaller than those of the generally bulk Bi_2Se_3 (thickness and size $\geq 10 \mu\text{m}$). That is to say, the as-synthesized “bulk” Bi_2Se_3 is nanosheet and not the real bulk Bi_2Se_3 . The higher E_g of as-synthesized “bulk” Bi_2Se_3 (1.08 eV) is attributed to the quantum size effect as also considered by Goror and Hodes⁵². Therefore, it is reasonable that the theoretical E_g of Bi_2Se_3 is smaller than the experimental E_g because the E_g growing is nearly inversely proportional to the lateral size⁵³.

For a 2D crystallite, the band gap shift, ΔE_g , is described by the equation^{54,55}

$$\Delta E_g = \frac{h^2}{4\mu_{xy}L_{xy}^2} + \frac{h^2}{8\mu_zL_z^2} \quad (2)$$

where μ_{xy} and μ_z are the reduced effective masses of electron-hole pairs in parallel (xy) and perpendicular (z) directions, respectively, and L_{xy} and L_z are the corresponding dimensions of the crystallite. For the ideally thin nanosheets, L_{xy} (0.1–1 μm) is much larger than L_z (0.96 nm for Bi_2Se_3 QL), so the first term in eq. 2 can be neglected. Consequently, the band gap shift depends only on L_z . As shown in Supplementary Fig. S12, we can get an approximate $\Delta E_g = E_g$ (13000 rpm) – E_g (bulk) = 0.42 eV. Therefore, the calculated μ_z is 0.24 m_e (m_e : electron mass). The Bohr radius R of exciton can be calculated by the following equation⁵⁶

$$R = \frac{\epsilon h^2}{\mu_z \pi e^2} \quad (3)$$

where ϵ is the dielectric constant at optical frequencies. The dielectric constant for Bi_2Se_3 can be typically set to be $100\epsilon_0$ ^{57,58}, where ϵ_0 is the vacuum permittivity. e is electron charge, 1.602×10^{-19} C. The calculated R from eq. 3 is about 21.79 nm. Therefore, the calculated R is much larger than the thickness of few-layer Bi_2Se_3 at 13000 rpm ($0.96 \times 2 = 1.92$ nm), suggesting that electron-hole pairs would be physically confined in few-layer Bi_2Se_3 . The calculated R values for other few-layer Bi_2Se_3 were listed in Supplement Table S1 and S2. It is well-known that semiconductors perform dramatic quantization effect when charge carriers (electrons and holes) are confined by potential barriers to small regions of space⁵⁹. Or equivalently, the thickness of few-layer Bi_2Se_3 is less than twice the Bohr radius of excitons in the bulk material. In a word, the blue-shift phenomenon implies that the E_g would increase with decreasing thickness, especially for the molecularly thin nanosheets by quantum size effect.

Under strong light excitation (Supplement Fig. S14), the electrons in the valence band become depleted while the final state in the conduction band is partially occupied, and further excitation from the valence band is blocked and no further absorption is induced, leading to a saturable absorption effect. The saturable intensity of few-layer Bi_2Se_3 thin film is much less than that of bulk Bi_2Se_3 (>50 layers). Therefore, the saturable absorption of few-layer Bi_2Se_3 is further exploited to Q-switch fiber laser, experimentally confirming the advantage of few-layer Bi_2Se_3 as a broadband saturable absorber because the Q-switching operation of as-synthesized bulk Bi_2Se_3 was extremely unstable with the large pulse-intensity and repetition-rate

fluctuation. Further exploiting the few-layer Bi_2Se_3 with the saturable absorption, we have successfully obtained the few-layer Bi_2Se_3 -based passive Q-switched EDFL. Compared with as-synthesized bulk Bi_2Se_3 , we have revealed that few-layer Bi_2Se_3 is more favorable for stable Q-switching. The reason why few-layer Bi_2Se_3 for Q-switched pulsed laser is superior to bulk Bi_2Se_3 could be explained as follows. It is well known that most of unique characteristics of topological insulator (including optical and electrical ones) originate from the metallic states on the surfaces or edges. As illustrated in Supplement Fig. S15, because bulk Bi_2Se_3 can be exfoliated to many few-layer Bi_2Se_3 sheets, in this process the surfaces/edges can be sharply increased. Therefore, one can think that the metallic states of few-layer Bi_2Se_3 should be stronger than that of bulk Bi_2Se_3 . As is well known, the electrons at the surface, such as metals, are very active with very low surface energy, and they are readily excited by externally electromagnetic (e.g. lightwave) or thermal fields. According to this way, one can easily understand that under light excitation, the surface electrons of few-layer Bi_2Se_3 can be transitioned more readily, because few-layer Bi_2Se_3 possesses more metallic surfaces/edges in comparison with the bulk one. Thus, the optically saturable absorption of few-layer Bi_2Se_3 is more excellent than that of bulk Bi_2Se_3 . Also, the few-layer Bi_2Se_3 can significantly enlarge the surface-to-volume ratio, and can be considered as a “quantum dot” that would result in quantum confinement. This could lead to the easier occurrence of the saturable absorption which has been partially verified by the lower saturable intensity (53 and 41 MW/cm²) in Fig. 5. Therefore, few-layer Bi_2Se_3 can generate the stable Q-switching operation compared to the unstable operation with bulk Bi_2Se_3 . The Q-switched laser based on few-layer Bi_2Se_3 has the low pump threshold of 9.3 mW, the pulse energy of 39.8 nJ, the pulse duration of 4.9 μs and the wide range of pulse-repetition-rate from 6.2 to 40.1 kHz, comparable to those reported fiber lasers Q-switched by other saturable absorbers (e.g. graphene⁶⁰, carbon nanotubes⁴⁴, and semiconductor^{38,39}). The promising results might have been due to the unique energy-band structure of few-layer Bi_2Se_3 . This performance of the Q-switched laser shows good prospects of few-layer Bi_2Se_3 as an excellently saturable absorber in the future.

Methods

Synthesis of bulk Bi_2Se_3 . Polyvinyl pyrrolidone (0.9 g) was dissolved in ethylene glycol (EG, 36 mL). Then bismuth oxide powder (Bi_2O_3 , 1 mmol), selenium powder (Se, 3 mmol) and ethylenediamine tetraacetic acid powder (4 mmol) were added into above-mentioned EG solution. The resulting suspension was stirred vigorously and subsequently sealed in a steel autoclave. The autoclave was heated to 200 °C in 30 min and maintained this temperature for 20 h. The as-obtained product was collected by high-speed centrifugation, washed several times with deionized water and absolute ethanol, and finally dried at 60 °C for 96 h in an oven.

Preparation of few-layer of Bi_2Se_3 . The as-synthesized bulk Bi_2Se_3 was dispersed in NMP or stock solution of chitosan (0.2 mg·mL⁻¹) that was prepared in 0.5% acetic acid aqueous solution at a concentration of 1 mg·mL⁻¹ by sonication in a sonic bath for 30 h (KQ–250 DB). The upper part of the resulting suspension after leaving to stand for 24 h was collected and centrifuged for 30 min at 1000 rpm. Subsequently, the supernatant was decanted to another centrifuge tube. After centrifuging the supernatant at 10000 rpm for 10 min, the as-obtained product was collected into phials and dispersed in the solvent used above for further characterization.

Characterization. Powder X-ray diffraction system (Rigaku Ultima IV XRD) equipped with Cu K α radiation ($\lambda = 1.542 \text{ \AA}$) over the 2θ range of 10–80° was used to characterize the crystal structure of as-synthesized bulk and few-layer Bi_2Se_3 . The sample was prepared by dropping the dispersive solutions on the surface of glass slide which had been etched a groove, then drying with an infrared lamp. Again and again to depositing a film on the fluted glass was named a continuous drop-dry process. SEM images were obtained on LEO-1530 operated at 20 kV. SEM samples were prepared by depositing a small drop of solution on small pieces of silicon wafer and then dried at room temperature. Energy dispersive X-ray spectrum pattern was acquired through spreading as-synthesized Bi_2Se_3 powders on sample stage directly. The micrographs of samples were taken using a transmission electron microscope (JEOL JEM-1400, JEM-2100) at an accelerating voltage of 200 kV. To prepare the TEM samples, a small drop of sample was deposited onto copper grids coating with lacey carbon film and then dried under room temperature at atmospheric pressure. AFM images were obtained in the tapping mode in air using an Agilent 5500 atomic force microscope. The samples were prepared by dropping their dispersions on mica



- substrates. Raman spectra (XploRA, Jobin-Yvon) were recorded with a diode laser at the excitation wavelength of 532 nm. The UV-vis absorption spectrum was measured on UV-vis spectrometer (UV-2550, Shimadzu). The UV-vis-NIR absorption spectrum was recorded on a Varian Cary 5000. The linear absorption spectra were measured by a spectrophotometer (Perkinelmer Lambda 7500) scanning from 300 to 2000 nm. The output laser spectrum was monitored by an optically spectral analyzer (Advantest Q8384) with the spectral resolution of 0.01 nm. The pulsed characteristics of this laser were detected by a 10 GHz photodetector (Nortel PP-10G) together with a digital storage oscilloscope (DSO, Agilent MSO7104A) and a radio-frequency (RF) spectrum analyzer (Gwinstek GSP-930).
- Moore, J. Topological insulators: the next generation. *Nat. Phys.* **5**, 378–380 (2009).
 - Moore, J. E. The birth of topological insulators. *Nature* **464**, 194–198 (2010).
 - Kong, D. & Cui, Y. Opportunities in chemistry and materials science for topological insulators and their nanostructures. *Nat. Chem.* **3**, 845–849 (2011).
 - Zhang, H. *et al.* Topological insulators in Bi₂Se₃, Bi₂Te₃ and Sb₂Te₃ with a single Dirac cone on the surface. *Nat. Phys.* **5**, 438–442 (2009).
 - Xia, Y. *et al.* Observation of a large-gap topological-insulator class with a single Dirac cone on the surface. *Nat. Phys.* **5**, 398–402 (2009).
 - Chen, Y. L. *et al.* Experimental realization of a three-dimensional topological insulator, Bi₂Te₃. *Science* **325**, 178–181 (2009).
 - Hsieh, D. *et al.* A tunable topological insulator in the spin helical Dirac transport regime. *Nature* **460**, 1101–1105 (2009).
 - Moore, J. & Balents, L. Topological invariants of time-reversal-invariant band structures. *Phys. Rev. B* **75**, 121306(R) (2007).
 - Hsieh, D. *et al.* Observation of unconventional quantum spin textures in topological insulators. *Science* **323**, 919–922 (2009).
 - Cao, H. L. *et al.* Quantized Hall effect and Shubnikov-de Haas oscillations in highly doped Bi₂Se₃: evidence for layered transport of bulk carriers. *Phys. Rev. Lett.* **108**, 216803 (2012).
 - Chen, X., Ma, X. C., He, K., Jia, J. F. & Xue, Q. K. Molecular beam epitaxial growth of topological insulators. *Adv. Mater.* **23**, 1162–1165 (2011).
 - Liu, H. T., Dai, J., Zhang, J. J. & Xiang, W. D. Solvothermal synthesis of Bi₂Se₃ hexagonal nanosheet crystals. *Adv. Mater. Res.* **236–238**, 1712–1716 (2011).
 - Xiu, F. *et al.* Manipulating surface states in topological insulator nanoribbons. *Nat. Nanotechnol.* **6**, 216–221 (2011).
 - Kong, D. *et al.* Topological insulator nanowires and nanoribbons. *Nano Lett.* **10**, 329–333 (2010).
 - Min, Y. *et al.* Surfactant-free scalable synthesis of Bi₂Te₃ and Bi₂Se₃ nanoflakes and enhanced thermoelectric properties of their nanocomposites. *Adv. Mater.* **25**, 1425–1429 (2013).
 - Qi, X. L. & Zhang, S. C. The quantum spin Hall effect and topological insulators. *Phys. Today* **63**, 33–38 (2010).
 - Sun, Y. *et al.* Atomically thick bismuth selenide freestanding single layers achieving enhanced thermoelectric energy harvesting. *J. Am. Chem. Soc.* **134**, 20294–20297 (2012).
 - Li, Y. Y. *et al.* Intrinsic topological insulator Bi₂Te₃ thin films on Si and their thickness limit. *Adv. Mater.* **22**, 4002–4007 (2010).
 - Peng, H. *et al.* Aharonov-Bohm interference in topological insulator nanoribbons. *Nat. Mater.* **9**, 225–229 (2010).
 - Li, H. *et al.* Controlled synthesis of topological insulator nanoplate arrays on mica. *J. Am. Chem. Soc.* **134**, 6132–6135 (2012).
 - Min, Y. *et al.* Quick, controlled synthesis of ultrathin Bi₂Se₃ nanodiscs and nanosheets. *J. Am. Chem. Soc.* **134**, 2872–2875 (2012).
 - Shahil, K. M. F., Hossain, M. Z., Goyal, V. & Balandin, A. A. Micro-Raman spectroscopy of mechanically exfoliated few-quintuple layers of Bi₂Te₃, Bi₂Se₃, and Sb₂Te₃ materials. *J. Appl. Phys.* **111**, 054305 (2012).
 - Novoselov, K. S. *et al.* Electric field effect in atomically thin carbon films. *Science* **306**, 666–669 (2004).
 - Hernandez, Y. *et al.* High-yield production of graphene by liquid-phase exfoliation of graphite. *Nat. Nanotechnol.* **3**, 563–568 (2008).
 - Lotya, M. *et al.* Liquid phase production of graphene by exfoliation of graphite in surfactant/water solutions. *J. Am. Chem. Soc.* **131**, 3611–3620 (2009).
 - Hasan, M. & Kane, C. Colloquium: topological insulators. *Rev. Mod. Phys.* **82**, 3045–3067 (2010).
 - Zarepour, P. *et al.* Proximity-induced high-temperature superconductivity in the topological insulators Bi₂Se₃ and Bi₂Te₃. *Nat. Commun.* **3**, 1056 (2012).
 - Bernard, F., Zhang, H., Gorza, S. P. & Emplit, P. Towards mode-locked fiber laser using topological insulators. *Nonlinear Photonics; 2012: Optical Society of America; 2012.*
 - Zhao, C. *et al.* Ultra-short pulse generation by a topological insulator based saturable absorber. *Appl. Phys. Lett.* **101**, 211106 (2012).
 - Tsai, T. Y., Fang, Y. C. & Hung, S. H. Passively Q-switched erbium all-fiber lasers by use of thulium-doped saturable-absorber fibers. *Opt. Express* **18**, 10049–10054 (2010).
 - Petropoulos, P. & Offerhaus, H. L. Passive Q-switching of fiber lasers using a broadband liquefying gallium mirror. *Appl. Phys. Lett.* **74**, 3619 (1999).
 - Keller, U. *et al.* Solid-state low-loss intracavity saturable absorber for Nd: YLF lasers: an antiresonant semiconductor Fabry-Perot saturable absorber. *Opt. Lett.* **17**, 505 (1992).
 - Hasan, T. *et al.* Nanotube-polymer composites for ultrafast photonics. *Adv. Mater.* **21**, 3874–3899 (2009).
 - Bao, Q. *et al.* Atomic-layer graphene as a saturable absorber for ultrafast pulsed lasers. *Adv. Funct. Mater.* **19**, 3077–3083 (2009).
 - Wang, Z., Lv, X. & Weng, J. High peroxidase catalytic activity of exfoliated few-layer graphene. *Carbon* **62**, 51–60 (2013).
 - Richter, W. & Becker, C. R. A Raman and far-infrared investigation of phonons in the rhombohedral V₂-VI₃ compounds Bi₂Te₃, Bi₂Se₃, Sb₂Te₃ and Bi₂(Te_{1-x}Se_x)₃ (0 < x < 1), (Bi_{1-y}Sb_y)₂Te₃ (0 < y < 1). *Phys. Status Solidi B* **84**, 619–628 (1977).
 - Zhang, J. *et al.* Raman spectroscopy of few-quintuple layer topological insulator Bi₂Se₃ nanoplatelets. *Nano Lett.* **11**, 2407–2414 (2011).
 - Zhao, C. *et al.* Wavelength-tunable picosecond soliton fiber laser with topological insulator: Bi₂Se₃ as a mode locker. *Opt. Express* **20**, 27888–27895 (2012).
 - Lu, S. *et al.* Third order nonlinear optical property of Bi₂Se₃. *Opt. Express* **21**, 2072–2082 (2013).
 - Sun, Z. *et al.* Graphene mode-locked ultrafast laser. *ACS Nano* **4**, 803–810 (2010).
 - Luo, Z. *et al.* Multiwavelength dissipative-soliton generation in Yb-fiber laser using graphene-deposited fiber-taper. *IEEE Photonics Technol. Lett.* **24**, 1539–1542 (2012).
 - Kelleher, E. *et al.* Nanosecond-pulse fiber lasers mode-locked with nanotubes. *Appl. Phys. Lett.* **95**, 111108 (2009).
 - Yamashita, S. *et al.* Saturable absorbers incorporating carbon nanotubes directly synthesized onto substrates and fibers and their application to mode-locked fiber lasers. *Opt. Lett.* **29**, 1581 (2004).
 - Zhou, D. P., Wei, L., Dong, B. & Liu, W. K. Tunable passively Q-switched erbium-doped fiber laser with carbon nanotubes as a saturable absorber. *IEEE Photonics Technol. Lett.* **22**, 9–11 (2010).
 - Zayhowski, J. & Kelley, P. Optimization of Q-switched lasers. *IEEE J. Quantum Electron.* **27**, 2220–2225 (1991).
 - Coleman, J. N. *et al.* Two-dimensional nanosheets produced by liquid exfoliation of layered materials. *Science* **331**, 568–571 (2011).
 - Trindade, T., O'Brien, P. & Pickett, N. Nanocrystalline semiconductors: synthesis, properties and perspectives. *Chem. Mater.* **13**, 3843–3858 (2001).
 - Ueda, K., Tabata, H. & Kawai, T. Magnetic and electric properties of transition-metal-doped ZnO films. *Appl. Phys. Lett.* **79**, 988 (2001).
 - Brus, L. A simple model for the ionization potential, electron affinity, and aqueous redox potentials of small semiconductor crystallites. *J. Chem. Phys.* **79**, 5566 (1983).
 - Henglein, A. Small-particle research: physicochemical properties of extremely small colloidal metal and semiconductor particles. *Chem. Rev.* **89**, 1861–1873 (1989).
 - Leutwyler, W., Bürgi, S. & Burg, H. Semiconductor clusters, nanocrystals, and quantum dots. *Science* **271**, 933–937 (1996).
 - Gorer, S. & Hodes, G. Quantum size effects in the study of chemical solution deposition mechanisms of semiconductor films. *J. Phys. Chem.* **98**, 5338–5346 (1994).
 - Vargas, A. *et al.* The Changing Colors of a Quantum-Confined Topological Insulator. *ACS Nano* **8**, 1222–1230 (2014).
 - Sandhoff, C., Hwang, D. & Chung, W. Carrier confinement and special crystallite dimensions in layered semiconductor colloids. *Phys. Rev. B* **33**, 5953–5955 (1986).
 - Smotkin, E. *et al.* Size quantization effects in cadmium sulfide layers formed by a Langmuir-Blodgett technique. *Chem. Phys. Lett.* **152**, 265–268 (1988).
 - Sakai, N., Ebina, Y., Takada, K. & Sasaki, T. Electronic band structure of titania semiconductor nanosheets revealed by electrochemical and photoelectrochemical studies. *J. Am. Chem. Soc.* **126**, 5851–5858 (2004).
 - Kim, D. *et al.* Surface conduction of topological Dirac electrons in bulk insulating Bi₂Se₃. *Nat. Phys.* **8**, 459–463 (2012).
 - Culcer, D., Hwang, E., Stanescu, T. & Sarma, S. Two-dimensional surface charge transport in topological insulators. *Phys. Rev. B* **82**, 155457 (2010).
 - Nozik, A. & Memming, R. Physical chemistry of semiconductor-liquid interfaces. *J. Phys. Chem.* **100**, 13061–13078 (1996).
 - Luo, Z. *et al.* Graphene-based passively Q-switched dual-wavelength erbium-doped fiber laser. *Opt. Lett.* **35**, 3709–3711 (2010).

Acknowledgments

This work is supported by the National Basic Research 973 Project (2014CB932004), National Natural Science Foundation of China (31371005, 81171453, 61107044), the Knowledge Innovation Program of Shenzhen City (JCYJ20130327150937484), the Fundamental Research Funds for the Central Universities, Program for New Century Excellent Talents in University, the Ministry of Education.

Author contributions

J.W., Z.Q.L. and L.P.S. conceived the work. Z.Q.L. performed the preparation experiments. J.P. assisted with characterization of materials. Y.Z.H. performed the optical experiment of fiber laser. All authors analyzed the data and prepared the manuscript.

Additional information

Supplementary information accompanies this paper at <http://www.nature.com/scientificreports>



Competing financial interests: The authors declare no competing financial interests.
How to cite this article: Sun, L.P. *et al.* Preparation of Few-Layer Bismuth Selenide by Liquid-Phase-Exfoliation and Its Optical Absorption Properties. *Sci. Rep.* 4, 4794; DOI:10.1038/srep04794 (2014).



This work is licensed under a Creative Commons Attribution-NonCommercial-NoDerivs 3.0 Unported License. The images in this article are included in the article's Creative Commons license, unless indicated otherwise in the image credit; if the image is not included under the Creative Commons license, users will need to obtain permission from the license holder in order to reproduce the image. To view a copy of this license, visit <http://creativecommons.org/licenses/by-nc-nd/3.0/>